Deuterium Kinetic Isotope Effects in the *p*-Side Pathway for Quinol Oxidation by the Cytochrome b_6f Complex[†,‡]

Glenda M. Soriano* and W. A. Cramer

Department of Biological Sciences, Purdue University, West Lafayette, Indiana 47907

Received July 13, 2001; Revised Manuscript Received October 9, 2001

ABSTRACT: Plastoquinol oxidation and proton transfer by the cytochrome b_6f complex on the lumen side of the chloroplast thylakoid membrane are mediated by high and low potential electron transport chains. The rate constant for reduction, k_{bred}, of cytochrome b_6 in the low potential chain at ambient pH 7.5−8 was twice that, k_{fred}, of cytochrome *f* in the high potential chain, as previously reported. k_{bred} and k_{fred} have a similar pH dependence in the presence of nigericin/nonactin, decreasing by factors of 2.5 and 4, respectively, from pH 8 to an ambient pH = 6, close to the lumen pH under conditions of steady-state photosynthesis. A substantial kinetic isotope effect, k_{H_2O}/k_{D_2O}, was found over the pH range 6−8 for the reduction of cytochromes b_6 and *f*, and for the electrochromic band shift associated with charge transfer across the b_6f complex, showing that isotope exchange affects the p*K* values linked to rate-limiting steps of proton transfer. The kinetic isotope effect, $k^{bred}_{H_2O}/k^{bred}_{D_2O} \approx 3$, for reduction of cytochrome *b* in the low potential chain was approximately constant from pH 6−8. However, the isotope effect for reduction of cytochrome *f* in the high potential chain undergoes a pH-dependent transition below pH 6.5 and increased 2-fold in the physiological region of the lumen pH, pH 5.7−6.3, where $k^{fred}_{H_2O}/k^{fred}_{D_2O} \approx 4$. It is proposed that a rate-limiting step for proton transfer in the high potential chain resides in the conserved, buried, and extended water chain of cytochrome *f*, which provides the exit port for transfer of the second proton derived from *p*-side quinol oxidation and a "dielectric well" for charge balance.

The cytochrome b_6f complex of oxygenic photosynthetic membranes couples electron transfer between the photosystem II and photosystem I reaction centers to the translocation of protons across the membrane and augmentation of the proton electrochemical potential, $\Delta\tilde{\mu}_{H^+}$ (*1*−*7*). Two protons per electron can be translocated by the b_6f complex to the electrochemically positive, *p*-side, aqueous lumen (*8*). The transfer of two electrons resulting from the oxidation of plastoquinol occurs in a "bifurcated" manner, through electron-transfer chains of high (positive) and low (negative) redox potential. Electron transfer to the low potential chain results from the "oxidant-induced reduction" by the quinol of the *p*-side heme of the cytochrome *b* subunit of the complex (Figure 1). This mechanism was initially proposed for the oxidation of ubiquinol by the cytochrome bc_1 complex in the mitochondrial respiratory chain (*9*, *10*), for which there are now high-resolution structure data (*11*−*14*), and in the photosynthetic bacterium *Rb. sphaeroides* (*15*). Structurally defined and distinct binding sites for Q_n- and Q_p-site quinone analogue inhibitors on opposite sides of the mitochondrial cytochrome bc_1 complex have been identified from the X-ray structures. The Rieske iron−sulfur protein is the immediate acceptor in the high potential chain for the quinol in the *p*-side binding niche. In the presence of the *p*-side[1] quinone analogue inhibitors, stigmatellin and myxothiazol, the iron−sulfur cluster of the Rieske ISP was found at a location proximal to either Q_p or to cytochrome c_1, the two sites separated by approximately 15 Å. In the Q_p-proximal position, one of the ligands of the 2Fe-2S cluster, His181-Nϵ2 in the yeast complex, is within a 2.8 Å H-bonding distance of O4 of stigmatellin (*13*, *14*), similar to that shown

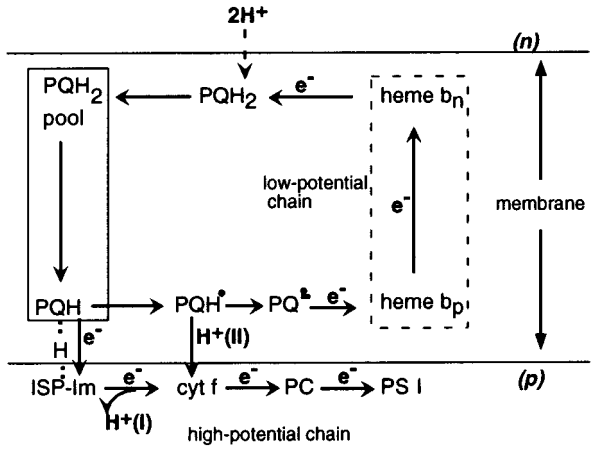

FIGURE 1: Bifurcated electron and proton transfer from plastoquinol to the high- and low-potential chains of the cytochrome b_6f complex. PQH_2 donates one hydrogen, H^+(I), in an H-bond with a deprotonated histidine ligand of the Rieske ISP, ISP−Im. The first proton, H^+(I), and first electron from quinol are transferred to ISP−Im. The pathways for transfer of the second electron and proton, H^+(II), must be different since upon reduction the ISP moves away from the quinol-proximal site. The neutral semiquinol, PQH•, is deprotonated before it is oxidized. The pathway of intramembrane transfer of H^+(II) is discussed in the text.

† This research has been supported by NIH Grant GM-38323 and the Henry Koffler Professorship from Purdue University.

‡ This manuscript is dedicated to the memory of our good friend and colleague, Jerry Babcock.

* To whom correspondence should be addressed: tel no (765) 494-2269; fax: (765) 496-1189; e-mail: gsoriano@purdue.edu.

10.1021/bi011465k CCC: $20.00
Published on Web 11/17/2001

in Figure 2. From this position of the bound quinol, there is no distance constraint for electron or proton transfer from the quinol to the ISP.

The neutral quinol does not have a sufficiently reducing potential to reduce the ISP (*17*, *18*). Therefore, deprotonation of the neutral quinol, $QH_2 \rightarrow QH^- + H^+$ (*19*), or transfer of one of its protons to a histidine (*20*) ligand of the ISP must be an initial step in the oxidation of quinol by the high and low potential chains. The transfer of the second electron would also be preceded by deprotonation of the semiquinone. This proton is subsequently transferred to the *p*-side aqueous phase. Thus, two protons can be transferred to the *p*-side aqueous phase for each electron transferred through the high potential chain. From spectroscopic data (*3*, *5*, *21*, *22*), and by analogy with the bc_1 complex, with which cytochrome b_6 has a large sequence and hydropathy similarity (*23*), and pronounced *p*-side sequence identity (*24*), the first electron released by plastoquinol (PQH_2) oxidation in the *p*-side quinol binding niche (Q_p) is inferred to be transferred to the ISP in the high potential chain. It would then be transferred to the higher potential carriers in the chain, ISP $\rightarrow$ cyt $f \rightarrow$ PC or cyt $c_6 \rightarrow$ PSI. The deprotonated semiquinone product, $PQ^{\bullet-}$, can transfer the second electron to heme b_p of cytochrome b_6 ("oxidant-induced reduction") in the low-potential chain. On the basis of the H-bond distance between stigmatellin and one of the histidine ligands of the ISP seen in the X-ray structure of the bc_1 complex, a model for the initial steps of *p*-side charge transfer in the oxidation of PQH_2 by the cytochrome b_6f complex can be summarized:

$$\text{(i)}\quad \text{ISP(ox)}\cdot\text{ImH}^+ \rightarrow \text{ISP(ox)}\cdot\text{Im} + \text{H}^+ \qquad (1)$$

$$\text{(ii)}\quad \text{PQH}_2 + \text{ISP(ox)}\cdot\text{Im} \rightarrow \text{PQH}^{\bullet}\cdots\text{ISP(red)}\cdot\{\text{Im}\}\text{H}^+$$

$$\text{(iii)}\quad \text{PQH}^{\bullet} \rightarrow \text{PQ}^{\bullet-} + \text{H}^+$$

$$\text{(iv)}\quad \text{PQ}^{\bullet-} + b_p(\text{ox}) \rightarrow \text{PQ} + b_p(\text{red})$$

The absence of an EPR signal associated with $PQH^{\bullet}$ has been attributed to antiferromagnetic coupling with the proximal reduced 2Fe-2S cluster (*25*). The location of the inhibitor, myxothiazol, in a niche closer to heme b_p than stigmatellin (*11*, *14*) implies the possibility of a second physiological quinone binding site, Q_{p2}, in addition to the Q_{p1} site occupied by stigmatellin (Figure 2). The myxothiazol binding niche could be filled under physiological conditions by movement of the semiquinone from the Q_{p1} site, or occupancy by a second *p*-side bound quinone (*19*, *26*). Although, electron transfer from a quinone/semiquinone in the stigmatellin site to heme b_p of the low potential chain (eq 1-iv) may be possible in terms of distance constraints

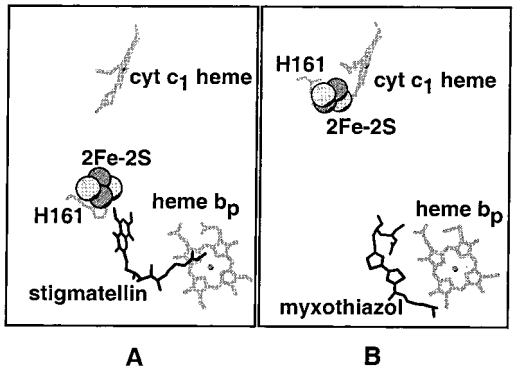

FIGURE 2: Structural basis of bifurcated charge transfer to the cytochrome bc_1 complex in chicken mitochondria. (A) In the presence of stigmatellin, the 2Fe-2S cluster is in the quinol-proximal site (*11*). (B) In the presence of myxothiazol, the 2Fe-2S cluster has moved away from the quinol site to a position closer to cytochrome c_1 (*11*, *12*). Structures drawn with MOLSCRIPT (*16*).

(*27*, *28*), the Q_p-heme b_p distance would be shorter from the site occupied by myxothiazol, and electron-transfer thus facilitated (*20*, *29*). Occupation of a Q_{p2} site by $PQH^{\bullet}$ or $PQH^{\bullet-}$ should allow detection of the semiquinone EPR signal unless the occupancy is very short-lived.

The above formulae describing the *p*-side charge transfer mechanism for quinol oxidation by high and low potential electron transfer chains imply that if *p*-side charge transfer between low and high potential chains is tightly coupled, or if the initial deprotonation of the quinol (eq 1-ii) is rate-limiting, the coupling of proton transfer to electron transfer should be the same or similar in the high and low potential chains. However, reduction of cytochrome *f* in the high potential chain of the cytochrome b_6f complex was found to be rate-limiting in mutants of cytochrome *f* in which the amino acids that H-bond to the cytochrome *f* internal water chain have been altered (*30*). This conserved extended internal water chain (*31*) has been proposed to be a *p*-side exit port for quinol-derived protons (*32*). This would provide a proton-transfer pathway unique to the high potential chain that is removed from the initial steps of charge separation at the Q_p site and could affect H^+-coupled electron transport in the high potential chain.

The coupling of H^+ and electron transfer in the high and low potential chains of the cytochrome b_6f complex in thylakoid membranes was studied under single flash conditions. Deuterium kinetic isotope effects, determined for the charge-transfer events in the cytochrome b_6f complex, imply that reductive electron transfer in cytochrome *f* is proton-coupled in the mildly acidic pH range that is physiological for the lumen side of the membrane.

METHODS

Isolation of Chloroplasts. Intact chloroplasts from store-bought or greenhouse-grown (Gurney's Seed and Nursery; Medania variety) spinach were isolated using the method given in ref *22*. The chloroplasts were suspended at a chlorophyll concentration of ~1−3 mg/mL in 10 mM Hepes/NaOH buffer, pH 7.6, 0.2 M sucrose, 30 mM KCl, 1 mM $MnCl_2$, 1 mM $MgCl_2$, 0.5 mM KH_2PO_4, 2 mM EDTA.

Flash Kinetic Spectroscopy. The rates of redox changes in cytochromes *f* and b_6, and the rate of generation of the slow phase of the electrochromic shift, $\Delta\Psi_s$, were measured

[1] Abbreviations: bR, bacteriorhodopsin; cyt, cytochrome; DBMIB, (2,5-dibromo-3-methyl-6-isopropyl-p-benzoquinone); DCCD, *N*,*N*′-dicyclohexylcarbodiimide; DCMU, 3-(3,4-dichlorophenyl)-1,1-dimethylurea; H^+(I), H^+(II); first and second protons derived from quinol deprotonation; ISP, iron−sulfur protein; ISP−ImH^+, iron−sulfur protein with a protonated histidine ligand; *n*, *p*, negative, positive sides of the transmembrane proton electrochemical potential gradient, $\Delta\tilde{\mu}_H^+$; NQNO, 2-*n*-nonyl-4-hydroxyquinoline-*N*-oxide; PC, plastocyanin; PQH_2, plastoquinol; PS, photosystem; $\Delta\Psi_s$, slow phase of the electrochromic bandshift; Q_n, Q_p, quinone binding sites on the electrochemically negative and positive sides of the membrane.

by flash-kinetic spectroscopy under single flash conditions that did not generate a significant pH gradient. Actinic light was provided by 5-μs flashes from a Xe lamp, while the weak measuring beam was generated by a tungsten lamp as described in ref *33*. An average of 36 traces, with a 2 s dark time between each data acquisition, was used for each measurement. The following wavelengths were used: (i) cytochrome *f* redox changes: $\Delta A = A_{554} - (2A_{545} + A_{572})/3$, (ii) cytochrome *b*: $\Delta A = A_{564} - A_{575}$, and (iii) slow phase of electrochromic bandshift, $\Delta\Psi_s$: $\Delta A = A_{515} - A_{515}^{DBMIB}$. A recording that consisted only of the slow component, $\Delta\Psi_s$, was obtained by subtracting the trace of the bandshift measured in the presence of 1 μM DBMIB added to the sample, from a sample in the absence of DBMIB. DBMIB, a Q_p-analogue inhibitor, blocks electron transfer from quinol to the ISP by binding at the Q_p site (*21*). Addition of DCMU and hydroxylamine eliminated the amplitude of the fast component arising from charge separation in PSII. The conditions for the different spectroscopic measurements were: chlorophyll concentration, 30 μg/mL; 20 mM KCl, 5 mM $MgCl_2$, 0.2 M sucrose, 400 μM duroquinol, 100 μM methyl viologen, and 10 mM buffer. Buffers: pH 5.5−6.0, MES; pH 7.0−7.4, Hepes; pH 8, 8.5, Tricine. A mixture of buffers was also used, and the pH was adjusted according to the experiment. The following uncouplers or inhibitors of electron transport were added to the reaction medium: (i) cytochrome *f* redox changes: 0.5 μM nonactin, 0.5 μM nigericin, (ii) cytochrome b_6: 0.5 μM nonactin, 0.5 μM nigericin, 0.5 μM NQNO, (iii) slow electrochromic phase, $\Delta\Psi_s$: 15 μM DCMU, 200 μM hydroxylamine, 0.5 μM nigericin.

H/D Exchange. Duroquinol was added to the D_2O buffer and incubated for 5 min, after which chloroplasts and inhibitors were added. Incubation of chloroplasts in the D_2O buffer for 10 min gave similar k_H/k_D values as did the 5-min incubation with duroquinol. Buffers in D_2O were prepared by adding 99.9% D_2O (Cambridge Isotopes) to solid reagents. The pD was adjusted by addition of NaOD (NaOH dissolved in D_2O), and the pD value was determined by adding 0.4 to the pH meter reading (*34*). This 0.4 correction has been shown to be correct for different electrolytes and pH values for mole fractions of ^2H higher than 0.90. The correction to the pH meter reading is dependent on the mole fraction of ^2H_2O or deuterium in the solvent, so that in mixtures of D_2O and H_2O, values of less than 0.4 should be used. An empirical equation for the correction, ΔpH_m, to pH meter measurements for different mole fractions, *m*, of deuterium is $\Delta pH_m = 0.076m^2 + 0.331m$ (*34*). In the current experiments, the mole fraction of deuterium is less than 1.00 because the solid reagents used are not deuterated, and the D_2O (99.9% deuterium) and the D_2O buffer in the cuvette are slightly diluted by the addition of chloroplast suspension. The smallest possible value for the ΔpH correction using the empirical equation above is about 0.376, close to 0.4 and within the measurement error of most pH meters.

Determination of Activation Energies, $\Delta G^{\ddagger}$. All measurements were done with a thermostated cuvette holder. The buffer was allowed to equilibrate with the temperature of the water bath for 20 min before use. A digital thermometer (Fisher Scientific) was used to measure the temperature of the sample inside the cuvette. $\Delta G^{\ddagger}$ was determined according to the formula, $k = Ae^{-\Delta G^{\ddagger}/RT}$, where *k* is the rate constant of the reaction, *A* is a preexponential factor, *R* the molar gas constant, and *T* the temperature in °K.

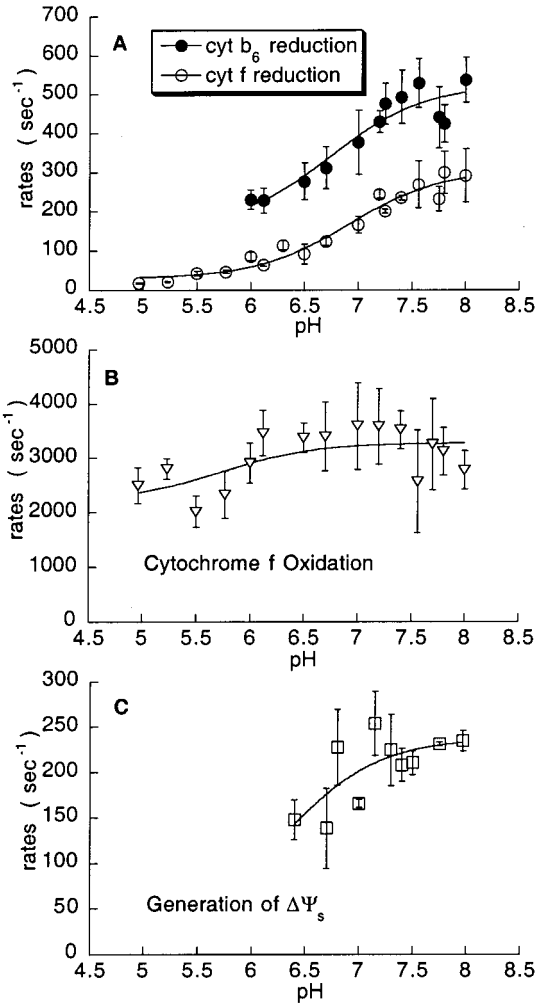

FIGURE 3: pH-dependence of (A) rates of light-induced reduction of cytochromes b_6 and *f* in chloroplasts, (B) oxidation of cytochrome *f*, and (C) generation of the slow phase of the electrochromic bandshift, $\Delta\Psi_s$. Reaction medium: pH buffers as described in Methods, 400 μM duroquinol, 100 μM methyl viologen, 0.5 μM nigericin, 0.5 μM nonactin, and 0.2 μM NQNO for measurement of cytochrome *b* reduction in panel A. Solid lines are fits to a Henderson−Hasselbalch-type equation which gave effective pK = 6.7 ± 0.2 and 6.9 ± 0.1 for the reduction of cytochromes b_6 and *f*, respectively. Error bars represent standard deviations (≥3 trials).

RESULTS

pH-Dependence of the Rates of Charge-Transfer Reactions in b_6f Complex. (A) Cytochrome Oxidation and Reduction. The rates of reduction of cytochrome b_6 initiated by a short light flash, and of the dark reduction of cytochrome *f* after its oxidation by the flash, have a qualitatively similar dependence on pH (Figure 3A). The rates of reduction of cytochromes b_6 and *f* decrease at acidic pH values and are smaller at pH 6 relative to pH 7.5−8 by a factor of 2.5 and 4, respectively. Because of the inability of the light flash to generate a transmembrane pH gradient and the presence of the ionophores nigericin and nonactin, the pH of the internal lumen and the external medium were equivalent. Thus, an ambient pH of 6 is close to the value of the lumen pH under conditions of steady-state photosynthesis (*35*).

A similar pH dependence for turnover of b_6f and bc_1 complexes has been observed for (i) cytochrome *f* reduction in chloroplasts, with the ratio of reductive rate constants at pH 8 and 6, $k_{cytf}^{(pH8)}/k_{cytf}^{(pH6)} \approx 2.7$ (*22*, *36*); (ii) the rate of steady-state electron transfer in isolated b_6f complex, $k_{cytf}^{(pH8)}/k_{cytf}^{(pH6)} \approx 5$ (*37*, *38*); (iii) the reduction of the low-potential (cytochrome *b*) chain of the cytochrome bc_1 complex of the bacterium, *Rb. sphaeroides* (*20*) with $k_{cytf}^{(pH8)}/k_{cytf}^{(pH6)} \approx 3$; (iv) the light-induced reduction of cytochrome c_1 in *Rb. sphaeroides* with $k_{cytf}^{(pH8)}/k_{cytf}^{(pH6)} \approx 3-4$ (*39*), and (v) the steady-state turnover of the cytochrome bc_1 complex isolated from yeast and mitochondria, with $k_{cytf}^{(pH8)}/k_{cytf}^{(pH6)} \approx 4-5$ (*19*).

Over the pH range used for measurement of the pH dependence of the reduction rate of cytochrome *f*, the rate of cytochrome *f* oxidation has a much smaller, but nonzero, pH-dependence (Figure 3B) below pH 6.5. The rate of the slow, millisecond electrochromic band-shift ($\Delta\Psi_s$) arising from electrogenic charge-transfer events in the cytochrome b_6f complex (*40*−*42*), has a pH-dependence similar to the reduction of cytochromes b_6 and *f* (Figure 3A,C) over the limited pH range where it could be measured (Figure 3C). A similar pH dependence of the $\Delta\Psi_s$ was observed in cells of the green alga, *Chlorella* (*43*).

No kinetics data are provided for cytochrome *b* reduction (Figure 3A) or the electrochromic band shift (Figure 3C) below pH 6.0, where their amplitudes are considerably smaller (Figure 4A,C), leading to a smaller signal-to-noise ratio and uncertain values of the rate constants. No significant change in amplitude was observed for cytochrome *f* turnover over this pH range (Figure 4B). The rate of cytochrome *b* reduction at all accessible pH values is always greater than that of cytochrome *f* (*22*, *30*), as has also been observed in *Chlorella* (*41*), indicating that the rate constant for reduction of cytochrome *f* does not necessarily indicate the true rate constant for transfer of the electron from plastoquinol to the ISP. The effective rate constant for transfer from the redox-competent quinol species to cytochrome *f* includes those for (i) transfer from quinol to the Rieske ISP docked at the Q_p site, (ii) movement through constrained diffusion of the soluble Rieske domain from the Q_p-proximal site to a site proximal to cytochrome *f*, and (iii) electron transfer of the ISP docked at the latter site to cytochrome *f*. The electron transfer rate is presumably rapid, $k_{et} \approx 10^5$ s^{-1}, by analogy with ISP−cytochrome c_1 system (*44*).

Effective p*K* values of 6.9 ± 0.1 and 6.7 ± 0.2 were obtained for the pH-dependence of the reduction of cytochromes *f* and b_6, respectively, after fitting the data to a Henderson−Hasselbalch equation (Figure 3A). These p*K* values, which are essentially similar for the reduction of the high- and low-potential chains, may reflect the p*K* of the oxidized Rieske ISP (*45*) or protonatable groups in the cytochromes. The p*K* for quinol deprotonation is too high (*18*) to account for the obtained p*K* values.

The activation energy over the temperature range of 5−30 °C for the reduction of cytochromes *b* and *f* in the pH range, 7−8.5, is approximately 30 kJ/mol and increased to 35 and 40 kJ/mol at pH 6 (data not shown), somewhat smaller than the values of 46−50 kJ/mol measured at pH 7.8 after an extended (300 ms) flash (*46*). This is comparable to the pH-independent activation energy of approximately 40 kJ/mol for the reduction of cytochromes *b* and c_1 in the bc_1 complex

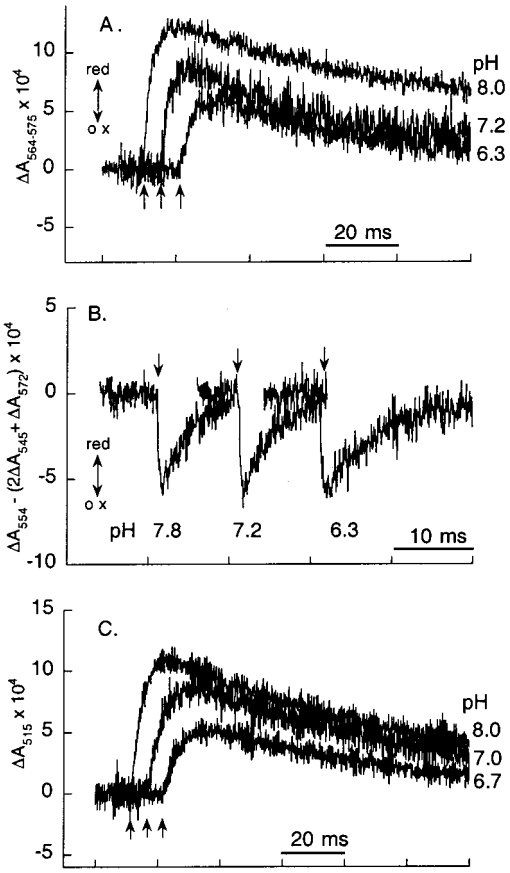

FIGURE 4: Amplitude as a function of pH of light-induced reduction of cytochromes b_6 (A) and *f* (B), and of the slow phase of the electrochromic bandshift, $\Delta\Psi_s$ (C). The kinetics traces were offset along the time axis. Arrows indicate direction of (A) reduction of cytochrome b6, (B) oxidation of cytochrome *f*, (C) generation of $\Delta\Psi_s$, and start of light flash. Reaction medium: pH buffers as described in Methods, 400 μM duroquinol, 100 μM methyl viologen, 0.5 μM nigericin, 0.5 μM nonactin, and 0.2 μM NQNO added for measurement of cytochrome *b* reduction.

from *Rb. sphaeroides* (*20*, *47*). The activation energy at pH 8.0 for the steady-state reduction of cytochrome *c* by the mitochondrial bc_1 complex was found to be approximately 30 and 44 kJ/mol for the bovine and yeast enzymes, respectively, for which a pH-dependence of −5.7 kJ/mol per unit pH change was reported (*19*).

Deuterium Kinetic Isotope Effects on Electron-Transfer Reactions of the Cytochrome b_6f Complex. A substantial kinetic isotope effect, k_{H_2O}/k_{D_2O}, was found over the pH range 6−8 for the reduction of cytochromes b_6, $k_{H_2O}/k_{D_2O} \approx 3$ (Figure 5A) and *f*, $k_{H_2O}/k_{D_2O} = 2-4$ (Figure 5B), and the microsecond electrochromic band shift $k_{H_2O}/k_{D_2O} \approx 2.5$ (Figure 5C). The plot of k_{H_2O}/k_{D_2O} vs pH or pD for cytochrome *f* reduction is best fit to a Henderson−Hasselbalch equation using an effective p*K* value of 6.4. This demonstrates that D/H isotope exchange affects the p*K* values linked to rate-limiting steps of proton transfer in both the low and high potential chains of the b_6f complex. Thus, it is inferred that pD values in the preparation of deuterated solvents can be determined by adding a correction of 0.4 to the measured value of pH as discussed above in Methods. The isotope effects were also independent of the time of incubation in deuterated buffers (*48*).

Reduction of Cytochrome b; *Electrochromic Bandshift*. The value of the deuterium kinetic isotope effect, $k_{H_2O}/k_{D_2O} \approx$

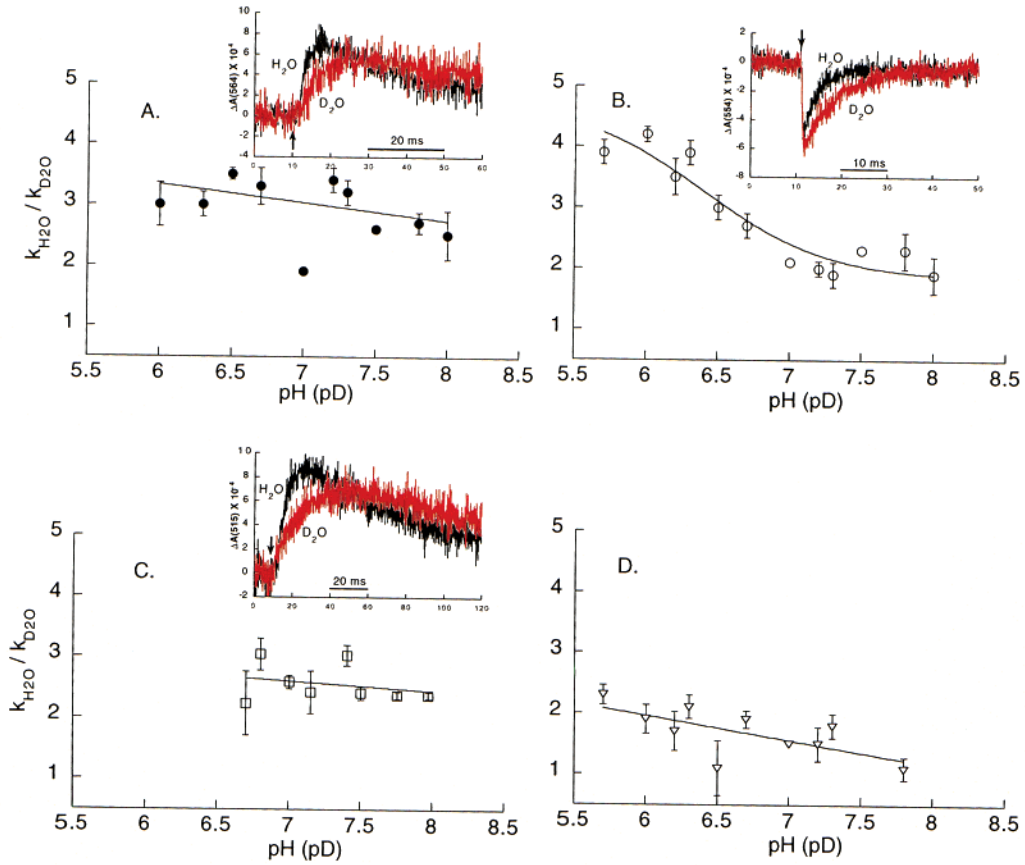

FIGURE 5: Deuterium isotope effect, k_{H_2O}/k_{D_2O}, as a function of pH(pD) for (A) cytochrome *b* reduction, (B) cytochrome *f* reduction, (C) generation of $\Delta\Psi_s$, and (D) cytochrome *f* oxidation. Inserted kinetics traces are for pH or pD = 7.2 for (A) cytochrome *b* reduction, (B) cytochrome *f* oxidation−reduction, and for pH or pD = 7.0 for (C) generation of $\Delta\Psi_s$. Black and red traces in each inset are for measurements in H_2O and D_2O, respectively. Arrows indicate start of light flash. The plot of k_{H_2O}/k_{D_2O} vs pH or pD for cytochrome *f* reduction is best fit to a Henderson−Hasselbalch equation using an effective p*K* value of 6.4 ± 0.2. Error bars represent standard deviations (≥3 trials).

3.0, for the reduction of cytochrome *b* in the low potential chain over the pH or pD range, 6−8, is slightly larger at acidic pH/pD values (Figure 5A). The kinetic isotope effect for the electrochromic bandshift, $k_{H_2O}/k_{D_2O} \approx 2.5$, is also approximately independent of pH over the range of possible measurements (Figure 5C), which extends only to pH 6.7 because of diminishing amplitude at lower pH values (Figure 4C). A kinetic isotope effect, $k_{H_2O}/k_{D_2O} = 1.4$, had been reported previously for the bandshift in spinach chloroplasts at pH/pD = 7.0 (*49*), and a value of 4.0 has been obtained from initial rates of the onset of $\Delta\Psi_s$ in whole cells of *C. reinhardtii* (*48*). Deuterated buffers caused a similar decrease in the amplitudes of cytochrome b_6 reduction and the generation of $\Delta\Psi_s$ (data not shown).

Oxidation and Reduction of Cytochrome f. The oxidation of cytochrome *f* in the high potential chain has a small kinetic isotope effect, $k_{H_2O}/k_{D_2O} \approx 1.3$, at pH 7.8, and a small monotonic pH dependence (Figure 5D). Values of $k_{H_2O}/k_{D_2O} < 1.4$ are most likely due to solvation effects and to differences in the physical properties of D_2O and H_2O (*34*). In contrast, the kinetic isotope effect for the reduction of cytochrome *f* undergoes a major increase on the acid side of pH 6.5−7.0 (Figure 5B). The kinetic isotope effect for reduction of cytochrome *f* increased 2-fold in the physiological pH region near pH 6, with $k^{fred}_{H_2O}/k^{fred}_{H_2O} \approx 4$ at pH 5.7−6.3. These values of the ambient pH are assumed to be very similar to those in the thylakoid lumen because of the presence of the ionophores nigericin and nonactin in the reaction medium. The small isotope effect obtained for the oxidation of cytochrome *f* is consistent with the results obtained with intact cells of *C. reinhardtii* (*48*).

DISCUSSION

1. Kinetic Isotope Effects. The use of D_2O as solvent in place of H_2O results in nonspecific isotopic substitutions because all readily exchangeable hydrogens such as those in O−H and N−H bonds will exchange rapidly with the deuterium in the solvent (*50*). Kinetic isotope effects on reaction rates are observed only if there are changes in bonding to the isotope that is actually undergoing transfer during the reaction. The effects on reaction rate arise as a result of a decrease in zero-point energy of the bond as H is replaced with the heavier ^2H (*34*). Factors such as the relative accessibility to solvent of the H-atoms in the protein will contribute to the observed solvent isotope effect (*34*, *50*). Hence, solvent isotope effects are often difficult to interpret on a mechanistic level, but can indicate the involvement of proton transfer in the overall reaction mechanism.

The presence of observable isotope effects on charge-transfer reactions within the cytochrome b_6f complex implies the coupling of proton and electron transfer, and that the rate-determining step can involve proton transfer. If the coupling of proton and electron transfer is the same for all the subsequent charge-transfer events, then one should expect to observe similar isotope effects for all the charge-transfer events within the b_6f complex. However, the pH or pD

dependence of the isotope effect for cytochrome *f* reduction (Figure 5B) is markedly different from that of the other charge transfer events (Figure 5A,C,D). A likely explanation is that in addition to deprotonation events common to the reduction of the high and low potential chains, additional deprotonation steps involving transfer of H^+(II) from $PQH^\bullet$ that are rate-limiting at pH 6 are also coupled to the reduction of cytochrome *f* (Figure 1).

2. Bifurcated Charge Transfer in the b_6f and bc_1 Complexes. The movement of the ISP [2Fe-2S] cluster from the Q_p-proximal site to the cyt c_1-proximal site upon reduction provides a physical basis for the bifurcated oxidation of the quinol (*11*). After the first proton, H^+(I), and electron are transferred from the quinol to the ISP, the soluble domain of the ISP undergoes a large scale rotation−translation from the Q_p-site and is no longer available to function as an acceptor for the second electron from the semiquinone, $PQH^\bullet$ or $PQ^{\bullet-}$. Thus, the semiquinone is not only thermodynamically competent to carry out reduction of the heme b_p, but this heme becomes the only available electron acceptor after the departure of the ISP from its binding site proximal to the Q_p binding niche. If it is assumed that the positions of stigmatellin and myxothiazol indicate the different positions of quinol and semiquinone, respectively, during electron and proton transfer to the Rieske ISP and to cytochrome *b*, the neutral semiquinone, $PQH^\bullet$, can move to a second site closer to heme b_p through lateral diffusion in the membrane, or by transfer to a neighboring quinone (*19*, *26*, *51*). The semiquinone, $PQH^\bullet$, would utilize a pathway for its deprotonation and transfer of H^+(II) to the *p*-side aqueous phase different from that through which the first proton is transferred (Figure 1). Thus, not only electron transfer, but proton transfer as well, can be bifurcated. The second proton would be transferred to the aqueous phase on the *p*-side of the membrane through intramembrane residues in cytochrome b_6, a chain or cluster of membrane-buried and -interfacial water molecules similar to those proposed in ref *47*, described in the structure of the yeast bc_1 complex (*14*); pdb #1EZV and, as suggested in the present work, through the cytochrome *f* intraprotein exit port (Figure 6). The scheme for charge-transfer reactions for the cytochrome b_6f complex proposed in the present study is similar to that inferred from the effects of DCCD on charge-transfer events in the b_6f complex (*52*), where bifurcation of H^+ transfer involves two *p*-side quinone binding sites.

The presence of a Q_p site and charge-transfer mechanisms in the cytochrome b_6f complex similar to those in the bc_1 complex is likely, despite the differences between cytochrome *f* and c_1 (*31*), because of the high degree of conservation of amino acids between the b_6f and bc_1 complexes on the *p*-side of the membrane (*24*). Thus, one can discuss the rate-determining steps in the *p*-side charge-transfer reactions of the complex.

3. *Sequence of Charge-Transfer Reactions in the b_6f Complex*. Electron and proton transfer from plastoquinol at the Q_{p1} site initiates the charge-transfer reactions in the b_6f complex [Figure 1, eq 1]. Deprotonation of the neutral PQH_2 likely involves transfer of the first proton, H^+(I), to the Rieske ISP along with the first electron (eq 1-ii). Charge transfer to the ISP (eq 1-ii) and to the low-potential heme b_p (eqs 1-iv) can be also be considered concerted.

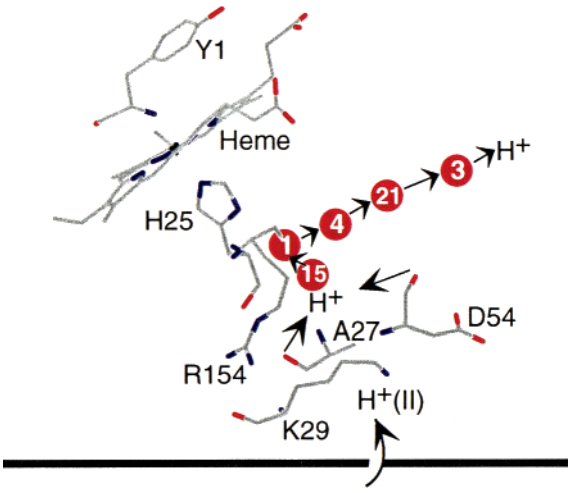

FIGURE 6: Proposed *p*-side lumenal exit pathway through cytochrome *f* for the second proton, H^+(II), released in the oxidation of PQH_2 (eq 1). Cytochrome *f* is tilted in the model so that the heme makes ~30° angle relative to the membrane plane. Transfer of H^+ from the membrane can occur through protonation of charged residues R154, K29, or D54 of cytochrome *f*. Also shown are the axial ligands of the heme Fe, Y1, and H25. The waters are shown as balls and are numbered according to pdb file 1HCZ. This figure was drawn with MOLSCRIPT (*16*).

Reduction of heme b_p by $PQ^{\bullet-}$ (eq 1-iv) is thermodynamically more favorable than by $PQH^\bullet$ (*53*), so deprotonation of $PQH^\bullet$ should occur prior to or concomitant with, electron transfer to heme b_p. Because, as observed in intact *C. reinhardtii* (*30*), as well as in spinach thylakoids [cf., Figures 3A, and also ref *22*)], the rate of cytochrome b_6 reduction is approximately 2-fold larger than that of cytochrome *f* [cf., Figure 3A above, and also refs *22*, *30*, *41*], the transfer of the second proton, H^+(II) from $PQH^\bullet$ is believed to precede reduction of cytochrome *f* (eqs 2-i,ii):

$$\text{(i)}\quad \text{cyt } f(\text{ox}) + H^+(\text{II}) \rightarrow \text{cyt } f(\text{ox})-H^+ \qquad (2)$$

$$\text{(ii)}\quad ISP^- + \text{cyt } f(\text{ox})-H^+ \rightarrow ISP + \text{cyt } f(\text{red})-H$$

or

$$\text{(iii)}\quad \text{cyt } f(\text{ox}) + e^- + H^+(\text{II}) \rightarrow \text{cyt } f(\text{red})-H$$

The larger deuterium isotope effect for cytochrome *f* reduction at lower pH implies that transfer of H^+(II) to cytochrome *f* either precedes (eqs 2-i, ii) or occurs in parallel with its reduction by the ISP (eq 2-iii). It is difficult to distinguish a sequential (eqs 2-i,ii) mechanism from one that is totally cooperative (eq 2-iii). The close coupling of electron and proton-transfer events in the cytochrome b_6f complex suggests that the description of tight coupling in simpler chemical systems may also apply to the cytochrome complexes (*54*).

4. Proposed Intraprotein Proton-Transfer Pathways. Transfer of the second proton, H^+(II), generated by the oxidation of quinol to the aqueous *p*-side space could occur through proton transfer from the semiquinone of *p*-side intramembrane polar amino acids and connected water molecules. These amino acids could be part of the transmembrane "proton channels" in the cytochrome b_6f complex as proposed in ref *52*. The internal water chain in cytochrome *f* could then provide the final exit pathway for the proton.

The highest resolution structural model for intramembrane water chains in H^+ transfer linked to energy transduction is that of bacteriorhodopsin (*55*). A *p*-side water chain has been described in the yeast cytochrome bc_1 complex (*14*) and was proposed earlier to participate in H^+ translocation across the membrane (*47*). In the latter model, an H-bond network at the Q_p site is formed by a histidine ligand of the 2Fe-2S cluster, water molecules, and side chains of Glu272 from cytochrome *b*. Another H-bond network around heme b_p is formed by water molecules, propionates of heme b_p, and side chains of cytochrome *b*. The chain of water molecules at this site lies in a pocket that is near the interface of cytochromes *b* and c_1.

5. H^+ Transfer into Cytochrome f. Regarding the mechanism of transfer of H^+(II) from the membrane interface into cytochrome *f*, if the heme of cytochrome *f* is tilted at ~30° with respect to the membrane plane, the H^+(II) could be taken up by protonatable residues on the surface of cytochrome *f*, from which the protons could access the water chain. The 75 Å long cytochrome *f* is expected to lie almost parallel to the membrane plane because in chloroplasts, the width of the lumenal space is only 40−90 Å with the larger dimension found during darkness (*56*, *57*). A cluster of charged residues, Lys29, Asp54, and Arg154, on the surface of cytochrome *f* and accessible to the water chain via Ala27, which H-bonds to one of the waters, could act as proton acceptors (Figure 6). However, the distances from the side chains of the charged residues are greater than the length of an H-bond. It would be necessary in the model that H^+ transfer be facilitated by side chain motion or the presence of intervening water molecules. There are precedents for side chain motion of significant amplitude. For example, (a) in the M state of bacteriorhodopsin, Cζ of the side chain of Arg82 moves toward the extracellular side, along the *c* axis, by 1.6 Å to function as both a proton donor and acceptor during the bR photocycle (*58*). (b) The position of the side chain of Glu272 in the bovine cytochrome bc_1 complex in the presence of stigmatellin is about 3.5 Å from its position in the absence of the inhibitor (*11*). The latter conformational change has been proposed to play a role in a *p*-side H^+ transfer similar to that described in the present work (*47*). It should be noted that the model for the transfer of H^+(II) to cytochrome *f* does not include a possible exit port from cytochrome *f* for this proton.

6. Proton Wires in Cytochrome f and Gramicidin A. A comparison can be made of the linear 5-water chain in cytochrome *f* with the 10-water linear chain of the gramicidin A channel. Like the water chain in cytochrome *f*, the single-file waters in the gramicidin A channel are interconnected through H-bonds and also make additional H-bonds with the polypeptide backbone (*59*). Proton transport along a proton wire has been modeled as a collective process of transfer of an ionic defect (an excess proton) followed by transfer of a bonding defect (reorientation of H-bonds) (*60*). Simulation of the dynamics of H^+ transfer through the gramicidin A channel has shown that this process occurs through a collective fluctuation of H-bond lengths along the chain and that proton conductance depends on the presence of well-connected H-bonds as well as flexibility of the chain. A water molecule can donate two H-bonds and accept two H-bonds via the two lone pairs of the O atom. The H-bonding network of cytochrome *f* (*31*) shows that all the H-bonds for the waters are "filled" except between two waters at the end of the chain. In the gramicidin channel, each water in the file has three H-bonds (two with its two neighbors and one with the protein backbone). On the basis of the structure of turnip cytochrome *f*, the average water−water (O−O) lengths are comparable to those in the gramicidin A channel (average of 2.6 Å). In cytochrome *f*, the extensive H-bonds with backbone amino acids in addition to the water−water bonds can decrease the flexibility of the chain relative to that in gramicidin. Given the saturation of the H-bonds in the 5-water proton wire of cytochrome *f*, how can an excess proton be transferred across this chain? The structure of cytochrome *f* may represent the structure in the presence of an excess proton. Propagation of this excess positive charge could take place through subtle changes in H-bond lengths. Also, the environment of the water chain in cytochrome *f* is not entirely nonpolar due to the presence of the heme. It is also likely that an excess negative charge on the heme Fe can facilitate proton translocation. Reorientation of the water chain is also necessary because the movement of the proton will cause dipoles to change direction. Before the next proton can enter the wire, the dipoles have to reorient. It has been shown that this reorientation can be rate-limiting in H^+ transfer (*59*). In cytochrome *f*, an incoming H^+ could cause the H-bonds to fluctuate or rearrange such that each O atom can be protonated. This seems plausible given the variable water−water and water−backbone H-bond lengths in cytochrome *f*.

7. Charge Neutralization Function of Cytochrome f Water Chain. As a mediator of proton-coupled electron transfer in cytochrome *f*, the water chain could also serve as a "dielectric well" (*61*). If the water chain provides the sole exit port for release of protons to the *p*-side bulk aqueous phase, then the functions of charge neutralization and terminal exit port are achieved through the same charge-transfer events. If there is an alternative exit port, then charge neutralization involving proton movement could be important in itself. In the latter case, the question would arise as to why cytochrome *f* requires a unique vectorially oriented 11 Å-long H_2O chain to accomplish the charge neutralization.

8. Cytochromes f and c_1. Because of the extensive lack of identity between cytochromes c_1 and *f* (*31*, *62*), a proton-transfer function for cytochrome c_1 analogous to that for cytochrome *f* discussed here would not necessarily be predicted. However, bound water molecules which might facilitate H^+ transfer are seen in cytochrome c_1 of the yeast bc_1 complex (*14*).

ACKNOWLEDGMENT

We are grateful to Prof. G. T. Babcock for several insightful comments and discussions.

REFERENCES

1. Velthuys, B. R. (1978) *Proc. Natl. Acad. Sci. U.S.A. 75*, 6031−6034.
2. Hope, A. B., and Rich, P. R. (1989) *Biochim. Biophys. Acta 975*, 96−103.
3. Joliot, P., and Joliot, A. (1994) *Proc. Natl. Acad. Sci. U.S.A. 91*, 1034−1038.
4. Kallas, T. (1994) in *The Molecular Biology of Cyanobacteria* (Bryant, D. A., Ed.) pp 259−317, Kluwer Academic Publishers, Dordrecht.

5. Kramer, D. M., and Crofts, A. R. (1994) *Biochim. Biophys. Acta 1184*, 193−201.
6. Cramer, W. A., Soriano, G. M., Ponomarev, M., Huang, D., Zhang, H., Martinez, S. E., and Smith, J. L. (1996) *Annu. Rev. Plant Physiol. Plant Mol. Biol. 47*, 477−508.
7. Hauska, G., Schütz, M., and Büttner, M. (1996) in *Oxygenic Photosynthesis: The Light Reactions* (Ort, D. R., and Yocum, C. F., Eds.) Kluwer Academic Publisher, Amsterdam.
8. Graan, T., and Ort, D. R. (1983) *J. Biol. Chem. 258*, 2831−2836.
9. Wikström, M. K. F., and Berden, J. A. (1972) *Biochim. Biophys. Acta 283*, 403−420.
10. Mitchell, P. (1975) *FEBS Lett. 59*, 137−139.
11. Zhang, Z., Huang, L., Shulmeister, V. M., Chi, Y. I., Kim, K. K., Hung, L. W., Crofts, A. R., Berry, E. A., and Kim, S. H. (1998) *Nature 392*, 677−84.
12. Iwata, S., Lee, J. W., Okada, K., Lee, J. K., Iwata, M., Rasmussen, B., Link, T. A., Ramaswamy, S., and Jap, B. K. (1998) *Science 281*, 64−71.
13. Kim, H., Xia, D., Yu, C. A., Xia, J. Z., Kachurin, A. M., Zhang, L., Yu, L., and Deisenhofer, J. (1998) *Proc. Natl. Acad. Sci. U.S.A. 95*, 8026−8033.
14. Hunte, C., Koepke, J., Lange, C., Robmanith, T., and Michel, H. (2000) *Structure 8*, 669−684.
15. Crofts, A. R., Meinhardt, S. W., Jones, K. R., and Snozzi, M. (1983) *Biochim. Biophys. Acta 723*, 202−218.
16. Kraulis, P. J. (1991) *J. Appl. Crystallogr. 24*, 946−950.
17. Rich, P., and Bendall, D. (1980) *Biochim. Biophys. Acta 592*, 506−518.
18. Rich, P. (1984) *Biochim. Biophys. Acta 768*, 53−79.
19. Brandt, U., and Okun, J. G. (1997) *Biochemistry 36*, 11234−11240.
20. Hong, S. J., Ugulava, N., Guergova-Kuras, M., and Crofts, A. R. (1999) *J. Biol. Chem. 274*, 33931−33944.
21. Malkin, R. (1982) *Biochemistry 21*, 2945−2950.
22. Heimann, S., Ponamarev, M. V., and Cramer, W. A. (2000) *Biochemistry 39*, 2692−2699.
23. Widger, W. R., Cramer, W. A., Herrmann, R. G., and Trebst, A. (1984) *Proc. Natl. Acad. Sci. U.S.A. 81*, 674−678.
24. Carrell, C. J., Schlarb, B. G., Bendall, D. S., Howe, C. J., Cramer, W. A., and Smith, J. L. (1999) *Biochemistry 38*, 9590−9599.
25. Jünemann, S., Heathcote, P., and Rich, P. R. (1998) *J. Biol. Chem. 273*, 21603−21607.
26. Ding, H., Robertson, D. E., Daldal, F., and Dutton, P. L. (1992) *Biochemistry 31*, 3144−3158.
27. Tezcan, F. A., Crane, B. R., Winkler, J. R., and Gray, H. B. (1999) *Proc. Natl. Acad. Sci. U.S.A. 98*, 5002−5006.
28. Page, C. C., Moser, C. C., Chen, X. X., and Dutton, P. L. (1999) *Nature 402*, 47−52.
29. Soriano, G. M., Ponamarev, M. V., Carrell, C. J., Xia, D., Smith, J. L., and Cramer, W. A. (1999) *J. Bioenerg. Biomem. 31*, 201−213.
30. Ponamarev, M. V., and Cramer, W. A. (1998) *Biochemistry 37*, 17199−17208.
31. Martinez, S., Huang, D., Ponamarev, M., Cramer, W. A., and Smith, J. L. (1996) *Protein Sci. 5*, 1081−1092.
32. Soriano, G. M., Smith, J. L., and Cramer, W. A. (2001) in *Handbook of Metalloproteins* (Messerschmidt, A., Huber, R., Wieghardt, K., and Poulos, T., Eds.) pp 172−181, Wiley, London.
33. Soriano, G. M., Ponamarev, M. V., Tae, G.-S., and Cramer, W. A. (1996) *Biochemistry 35*, 14590−14598.
34. Schowen, K. B. J. (1978) in *Transition States of Biochemical Processes* (Gandour, R. D., and Schowen, R. L., Eds.) Plenum Press, New York.
35. Kramer, D. M., Sacksteder, C. A., and Cruz, J. A. (1999) *Photosynth. Res. 60*, 151−163.
36. Nishio, J. N., and Whitmarsh, J. (1993) *Plant Physiol. 101*, 89−96.
37. Bendall, D. S. (1982) *Biochim. Biophys. Acta 683*, 119−151.
38. Hurt, E. C., and Hauska, G. (1981) *Eur. J. Biochem. 117*, 591−599.
39. Bashford, C. L., Prince, R. C., Takamiya, K.-I., and Dutton, P. L. (1979) *Biochim. Biophys. Acta 545*, 223−235.
40. Joliot, P., Delosme, R., and Joliot, A. (1977) *Biochim. Biophys. Acta 459*, 47−57.
41. Joliot, P., and Joliot, A. (1985) *Biochim. Biophys. Acta 806*, 398−409.
42. Jones, R. W., and Whitmarsh, J. (1985) *Photochem. Photobiol. 9*, 119−127.
43. Finazzi, G., and Rappaport, F. (1998) *Biochemistry 37*, 9999−10005.
44. Sadoski, R. C., Engstrom, G., Tian, H., Zhang, L., Yu, C. A., Yu, L., Durham, B., and Millett, F. (2000) *Biochemistry 39*, 4231−4236.
45. Zhang, H., Carrell, C. J., Huang, D., Sled, V., Ohnishi, T., Smith, J. L., and Cramer, W. A. (1996) *J. Biol. Chem. 271*, 31360−31366.
46. Whitmarsh, J., and Cramer, W. A. (1979) *Biophys. J. 26*, 223−234.
47. Crofts, A. R., Hong, S. J., Ugulava, N., Barquera, B., Gennis, R., Guergova-Kuras, M., and Berry, E. A. (1999) *Proc. Natl. Acad. Sci. U.S.A. 96*, 10021−10026.
48. Deniau, C., and Rappaport, F. (2000) *Biochemistry 39*, 3304−3310.
49. Farineau, J., Garab, G., Horvath, G., and Faludi-Daniel, A. (1980) *FEBS Lett. 118*, 119−122.
50. Connors, K. A. (1990) *Chemical Kinetics. The Study of Reaction Rates in Solution*, VCH Publishers, New York.
51. Sharp, R. E., Palmitessa, A., Gibney, B. R., White, J. L., Moser, C. C., Daldal, F., and Dutton, P. L. (1998) *Biochemistry 38*, 3440−3446.
52. Joliot, P., and Joliot, A. (1998) *Biochemistry 37*, 10404−10410.
53. Brandt, U. (1996) *FEBS Lett. 387*, 1−6.
54. Cukier, R. I., and Nocera, D. G. (1998) *Annu. Rev. Phys. Chem. 49*, 337−369.
55. Luecke, H., Richter, H. T., and Lanyi, J. K. (1998) *Science 280*, 1934−1937.
56. Whitmarsh, J. (1986) in *Encyclopedia of Plant Physiology: New Series: Photosynthesis III* (Staehelin, L. A., and Arntzen, C. J., Eds.) pp 508−527, Springer-Verlag, Berlin.
57. Haehnel, W. (1984) *Annu. Rev. Plant Physiol. 35*, 659−693.
58. Luecke, H., Schobert, B., Richter, H.-T., Cartailler, J.-P., and Lanyi, J. K. (1999) *Science 286*, 255−260.
59. Pomes, R., and Roux, B. (1996) *Biophys. J. 71*, 19−39.
60. Pomes, R., and Roux, B. (1998) *Biophys. J. 75*, 33−40.
61. Jünemann, S., Meunier, B., Gennis, R. B., and Rich, P. R. (1997) *Biochemistry 36*, 14456−14464.
62. Martinez, S. E., Huang, D., Szczepaniak, A., Cramer, W. A., and Smith, J. L. (1994) *Structure 2*, 95−105.

BI011465K